7 ENSO atmosphere and ocean feedback mechanisms

Suggested Literature:

a) Gill, A. E., 1980: 'Some simple solutions for heat-induced tropical circulation', *Quart. J. R. Met. Soc.*, **106**, 447-462.

b) Reference for reduced gravity model in oceans:
'Ocean Circulation' by R. X. Huang, *University Press, Cambridge*, 791 pp.

c) Online textbooks:
oceanworld.tamu.edu/resources/ocng_textbook/contents.html
oceanworld.tamu.edu/resources/oceanography-book/contents.htm

d) 'El Nino, La Nina, and the Southern Oscillation' by S. G. Philander, *Academic Press, INC.*, 293 pp.

e) For the ocean simulations presented:
Chang, P., 1994: 'A study of the seasonal cycle of sea surface temperature in the tropical Pacific Ocean using reduced gravity models', *J. Geophy. Res.*, **99**, C4, 7725-7741

7.1 Some general observations

Lets consider the sea surface temperature anomaly on 26th November, 2015 (Fig. 20). It's a manifestation of an El Nino development in the year 2015. Let's try to understand what is going on in the Pacific region.

The typical equatorial Pacific background state is shown in Fig. 21, in a vertical-zonal section. As can be seen it gets colder as we go from the surface downward (why?). And it also gets colder if we go from west to east. Looking at a map of sea surface temperature (SST), we see this equatorial asymmetry clearly (Fig. 22).

A schematic what is the situation in normal conditions (or La Nina) is given in 23. Trade winds are blowing near the equator from east to west (the reason theses trade winds will be discussed later in this course, but briefly it is due to the maximum convective heating that occurs in the mean around the equator). These trade winds push the warm surface waters to the west. What is happening then in the east?

However, there is an additional *Bjerknes* feedback mechanism working at the equator, which even further strengthens the equatorial easterly winds as shown in Fig. 24.

In El Nino conditions (Fig. 26) this normal situation breaks down and we get to a situation where also the eastern Pacific is flushed with warm waters (intuitively one would think that this is the 'normal' situation).

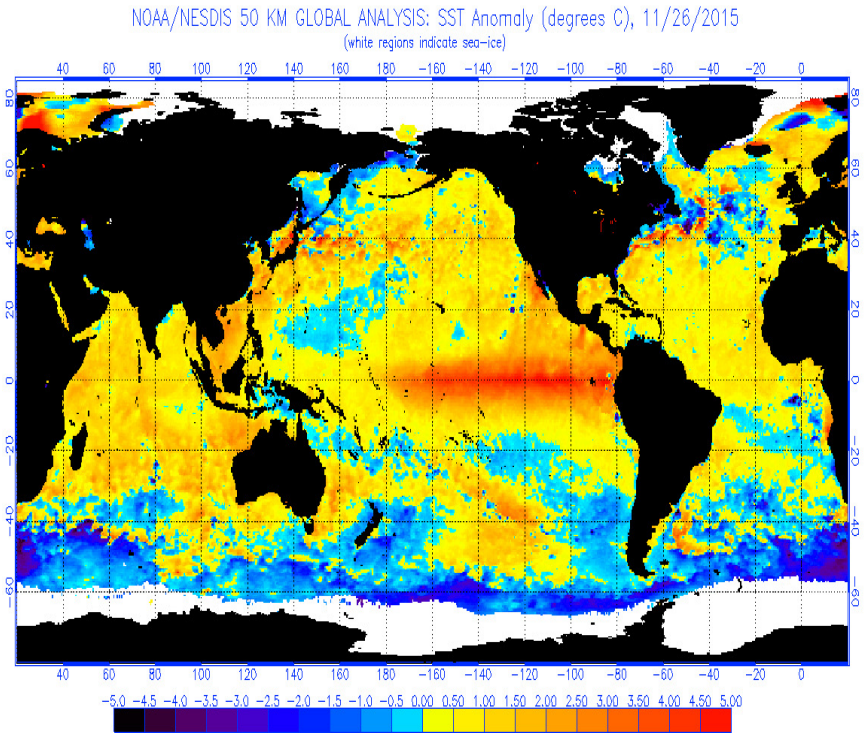

Figure 20: SST anomaly on 26. Nov 2015. Source: http://www.ospo.noaa.gov/data/sst/anomaly/2015/anomnight.11.26.2015.gif.

7.2 Atmospheric (ENSO) Teleconnections

In winter 2015/2016 one of the largest El Nino event in recent history happened (Fig. 27).

Such an ENSO event is considered to be the major source of seasonal predictability due to ENSO teleconnections Fig. 28.

In this section the physical basis for atmospheric teleconnections induced by tropical SST anomalies will be briefly discussed. How can we understand the origin of these teleconnections? Assuming we have an area warm SST anomalies. How do we assess what are the atmospheric adjustment processes. Surely a warm area of SST's will modify the stability of a parcel (see Fig. 29), but how exactly?

Note that the parcels that are considered here are much smaller in scale (1km) compared to the large-scale flow adjustments that we want to understand eventually. From the Atmospheric Physics course in the last term you know that for a moist, saturated parcel to be unstable the following criterion has to be fulfilled:

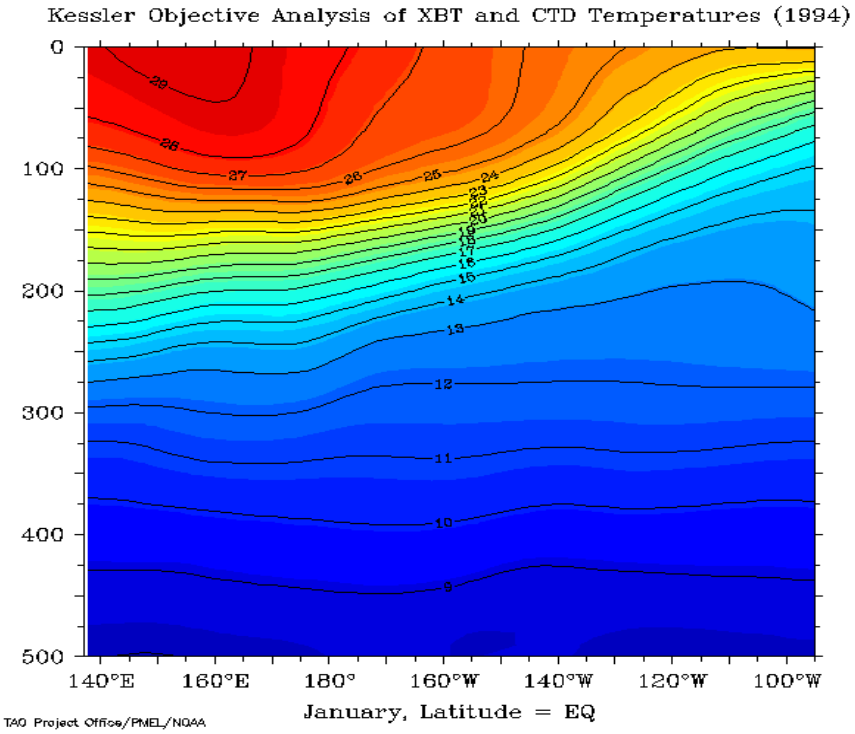

Figure 21: Average January temperature as a function of depths and longitude along the equator. Map from Pacific Marine Environmental Laboratory of NOAA, Seattle.

$$\frac{\partial \overline{T}}{\partial z} \leq -\frac{g}{c_p} \frac{\left(1 + \frac{L_{lv} m_{vs}}{RT}\right)}{\left(1 + \frac{L_{lv}^2 \overline{m}_{vs}}{c_p T^2 R_v}\right)} , \tag{192}$$

where quantities refer to the large-scale environment. As long as the parcel is not saturated the stability condition governed by the dry adiabate by setting m_{vs} to zero. This means that a warm surface would favour unstable conditions (Fig. 30).

For the moist saturated adiabatically rising parcel we have

$$\frac{dT}{dt} = -w \frac{g}{c_p} \frac{\left(1 + \frac{L_{lv} m_{vs}}{RT}\right)}{\left(1 + \frac{L_{lv}^2 m_{vs}}{c_p T^2 R_v}\right)} \quad . \tag{193}$$

Again, we can recover the unsaturated case by setting m_{vs} to zero, and this leads to the dry adiabatic lapse rate. This means the parcel always cools! It can be shown (see section 3.4) that due to the decreasing temperature the Relative Humidity (RH) of a rising, unsaturated parcel always increases until saturation is reached

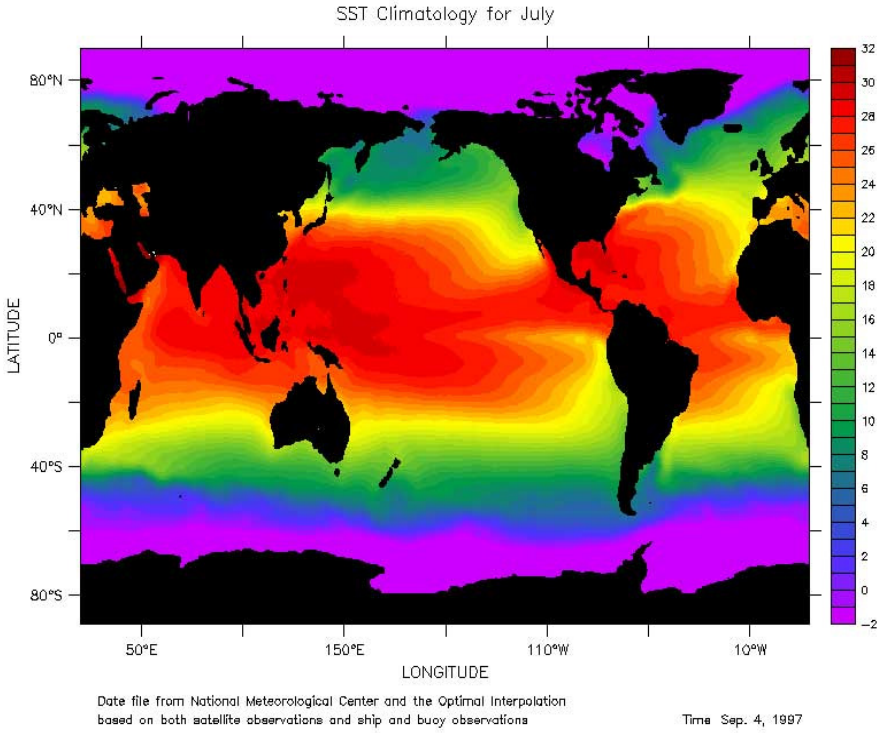

Figure 22: Mean sea-surface temperature calculated from the optimal interpolation technique (Reynolds and Smith, 1995) using ship reports and AVHRR measurements of temperature.

$$\frac{dRH}{dt} = -\frac{m_v}{m_{vs}^2}\frac{dm_{vs}}{dt} \geq 0 \quad , \tag{194}$$

If the parcel is rising further then condensation will occur. If the parcel raises far enough then nearly all its moisture may condensate and fall out as rain. This leads to diabatic heating of the atmosphere. In an unstable environment this leads to a huge asymmetry between rising and sinking parcels, because the sinking parcel may just evaporate the little moisture content in it. Note that if no rainfall is occurring, then the process of rising (condensation) and sinking (evaporation) would be reversible (no Entropy generation). It is the net heating related to the falling rain that makes the convection process irreversible. See also Foehn effect mechanism (Fig. 31).

As a net effect there is a large-scale tropospheric convective heating due to the SST-induced unstable conditions. From the thermodynamic equation (e.g. 135), we know that this will lead to further adjustments. In particular, for tropical regions we may assume that horizontal and time derivatives are negligible. We get the

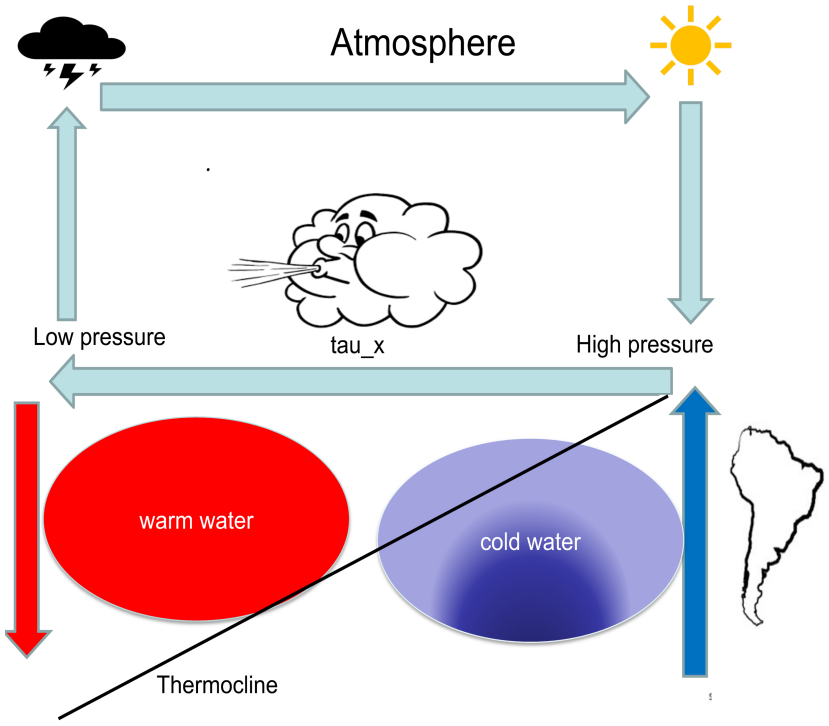

Figure 23: Normal conditions in the Pacific with strong trade winds pushing surface water toward the west and heavy rain in the west driving the atmospheric circulation.

approximate relations

$$\omega \approx -\rho g w \approx -\frac{Q}{c_p}\frac{1}{S_p} \tag{195}$$

or

$$w \approx \frac{Q}{c_p}\frac{1}{S_p \rho g} \quad . \tag{196}$$

This relation may also be applied to perturbations of Q and w.

$$\Delta w \approx \frac{\Delta Q}{c_p}\frac{1}{S_p \rho g} \quad , \tag{197}$$

if we assume that perturbations of S_p and ρ are small. It follows that increased heating in the region of warm SST anomalies has to be compensated by rising motion. Further adjustments may be explained by continuity as illustrated in Fig. 32.

For ENSO this could look like in Fig. 33. The signal in the upper troposphere may be spread through equatorial Rossby and Kelvin waves, and the resulting upper-level divergence may act as a Rossby-wave source in the vorticity equation 109.

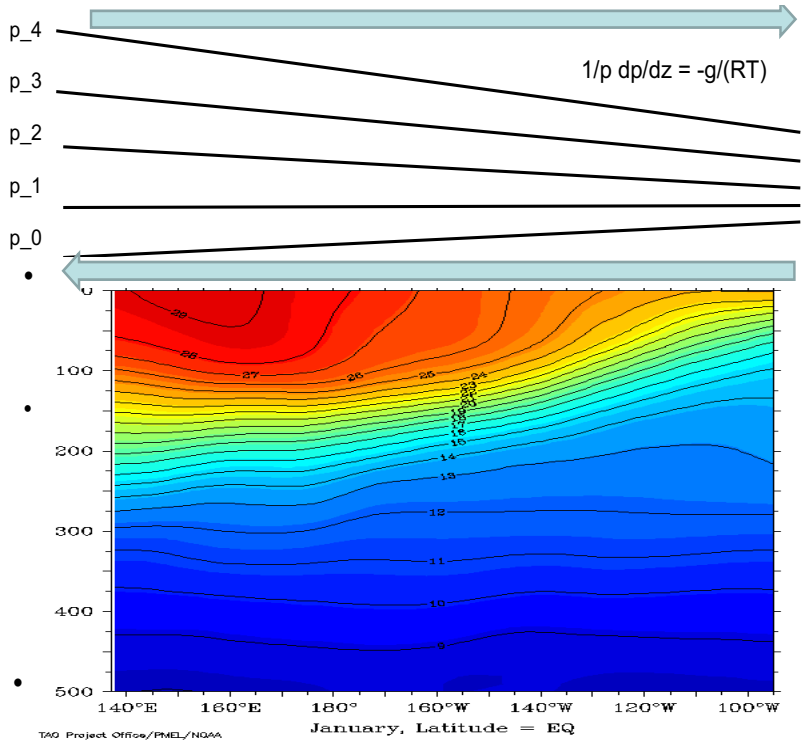

Figure 24: Cold conditions in east and warm conditions in west increase trade winds further due to the hydrostatic equation.

The typical sea surface temperature anomaly for an El Nino event is shown in Fig. 34. A warming of typically more than 1K is occurring in the eastern Pacific and surrounded by a cooling (so-called *Horse-shoe pattern*).

Fig. 35 shows the typical (composite) response of the atmosphere (rainfall [or heating!], and low-level winds) to the typical (composite) El Nino SST anomaly of Fig. 34.

The response in the central equatorial Pacific is a *weakening* of the trade winds, which is the positive atmospheric feedback, because a initial warm anomaly in the eastern Pacific will cause a response that is strengthening the original SST anomaly (why?). What is the typical period of ENSO? We will try to understand this local atmospheric response and the subsequent ocean response in the following subsections from a more theoretical point of view.

7.3 Atmospheric response to SST or heating anomaly

Kelvin and equatorial Rossby-gravity waves are also relevant for shaping the stationary response to an equatorial heating, so-called Gill response (Gill, 1980). In

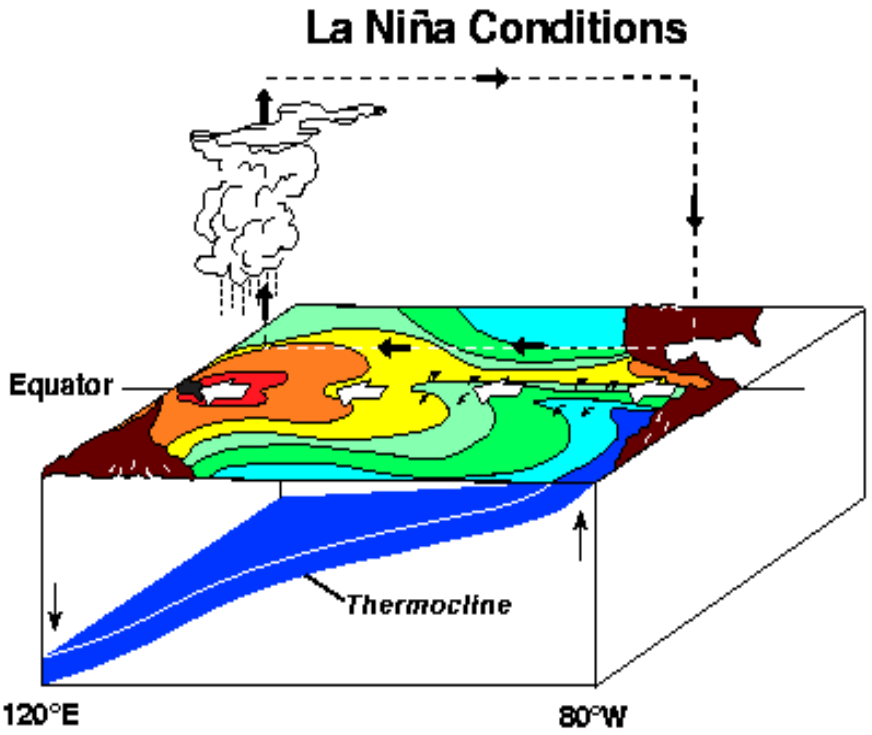

Figure 25: La Nina conditions in the Pacific with strong trade winds (black arrows) pushing surface water toward the west (white arrows) and heavy rain in the west driving the atmospheric circulation (black arrows). Colors give temperature of the ocean surface, red is hottest, blue is coldest. From: NOAA Pacific Marine Environmental Laboratory.

the Gill model a simple parameterization of the effect of heating on divergence, Q, is added to the continuity equation (in the Gill's paper and references therein proper justifications for this approach are presented)

$$\frac{\partial u'}{\partial t} = -\frac{\partial \Phi'}{\partial x} + \beta y v' \tag{198}$$

$$\frac{\partial v'}{\partial t} = -\frac{\partial \Phi'}{\partial y} - \beta y u' \tag{199}$$

$$\frac{\partial \Phi'}{\partial t} = -gh_e\left(\frac{\partial u'}{\partial x} + \frac{\partial v'}{\partial y}\right) - Q \ , \tag{200}$$

Finally, rayleigh friction and Newtonian cooling are added to the equations by replacing the time derivatives $\partial/\partial t$ by $\partial/\partial t + \ \epsilon$, and the equations are solved for a stationary state. The result of the (complicated) computations are illustrated in Fig. 36. To the west of the heating, we find the Rossby-gravity wave-type response,

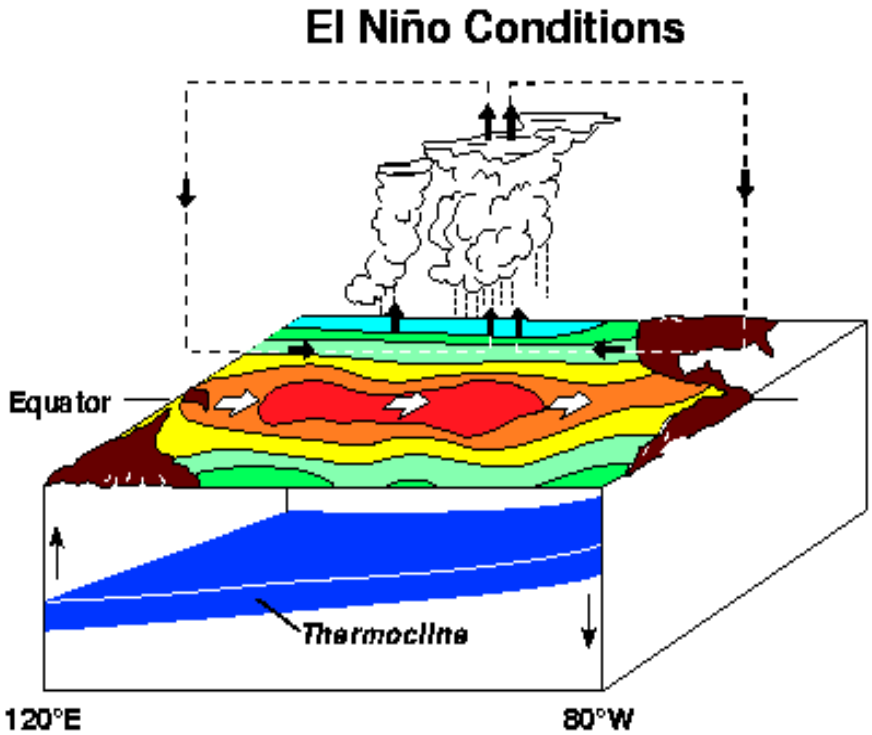

Figure 26: El Niño conditions in the Pacific with weak or reversed trade winds in the west (black arrows) allowing surface water to surge eastward (white arrows) and with heavy rain in the central equatorial Pacific driving the atmospheric circulation (black arrows). Colors give temperature of the ocean surface, red is hottest, blue is coldest. From: NOAA Pacific Marine Environmental Laboratory.

to the east we find the Kelvin wave-type response. Note that the Gill model is used, for example, to explain the atmospheric part of the positive (Bjerknes) feedback that leads to the ENSO phenomenon. Also note that a positive 'heating' Q explains the low-level convergent motions, but not the upper level ones (one would have to change sign to explain the upper-level response; upper-level divergence in case of a positive heating! Discuss!).

7.4 Response in the equatorial Ocean

7.4.1 Reduced gravity model

In this subsection we want to derive the equatorial ocean response to an atmospheric forcing of the Gill-type. If we consider the mean stratification of the equatorial Pacific Ocean of Fig. 21, one sees that warm water is residing on top of colder waters, divided by the thermocline. The simplest model of the upper Pacific are assuming therefore that there are 2 layers, divided by a density jump. Let layer 2 be the lower layer of density ρ_2 and height h_2, and the upper layer be of density ρ_1 and

height h_1. The aim here is to derive the pressure gradient force in the upper layer in this situation. We derive the pressure gradient force by integrating the hydrostatic equation 156 first in layer 2 from an arbitrary vertical position to the boundary h_2

$$\begin{aligned} \int_z^{h_2(x,y,t)} \frac{\partial p_2}{\partial z} dz &= -\int_z^{h_2(x,y,t)} \rho_2 g dz \ , \quad \text{or} & (201) \\ p_2(h_2) - p_2(x,y,z,t) &= -\rho_2 g[h_2(x,y,t) - z] \ . & (202) \end{aligned}$$

Then we apply the horizontal gradient

$$\nabla p_2(h_2) = \nabla p_2(x,y,t) - \rho_2 g \nabla h_2(x,y,t) \quad , \tag{203}$$

noting that the horizontal pressure gradient is independent on the vertical position.

Next we integrate further in layer 1

$$\begin{aligned} \int_{h_2(x,y,t)}^{z} \frac{\partial p_1}{\partial z} dz &= -\int_{h_2(x,y,t)}^{z} \rho_1 g dz \ , \quad \text{or} & (204) \\ p_1(x,y,z,t) - p_1(h_2) &= -\rho_1 g[z - h_2(x,y,t)] \ . & (205) \end{aligned}$$

We again apply the horizontal gradient

$$\nabla p_1(x,y,t) = \nabla p_1(h_2) + \rho_1 g \nabla h_2(x,y,t) \quad , \tag{206}$$

Continuity demands that $p_1(h_2) = p_2(h_2)$, therefore inserting 206 into 203 leads to:

$$\nabla p_1(x,y,t) = \nabla p_2(x,y,t) - (\rho_2 - \rho_1) g \nabla h_2(x,y,t) \quad . \tag{207}$$

Assuming the lower layer motionless and without pressure gradient $\nabla p_2(x, y.t) = 0$ and $H = h_1 + h_2 = const$ (rigid lid; an approximation here), and therefore $\nabla h_1 = -\nabla h_2$ we get

$$\nabla p_1(x,y,t) = (\rho_2 - \rho_1) g \nabla h_1(x,y,t) \quad , \tag{208}$$

or

$$\frac{1}{\rho_1} \nabla p_1(x,y,t) = \frac{\rho_2 - \rho_1}{\rho_1} g \nabla h_1(x,y,t) \quad . \tag{209}$$

The pressure gradient in the upper layer can be, to a first approximation, expressed in terms of the change in density between lower and upper layer and the gradient of the *thermocline depth* h_1. Since with respect the standard one-layer case the factor g is replaced by $(\rho_2 - \rho_1)/\rho_1 g = g'$, this model is called *reduced gravity model*. The density change $(\rho_2 - \rho_1)/\rho_1$ is typically about 1%. The *reduced gravity model* is identical to the shallow water equations, but with the pressure gradient force 209, because if the slight change of density between the 2 layers. We add a wind-stress forcing on the rhs of the following equations to mimic the ocean forced case. These equations are similar to the atmospheric Gill model, but with forcing in the momentum equations instead of in the continuity equation.

$$\frac{\partial u}{\partial t} + (\mathbf{u} \cdot \nabla)u = -g' \frac{\partial h}{\partial x} + fv + \frac{1}{\rho h}\tau_x \quad (210)$$

$$\frac{\partial v}{\partial t} + (\mathbf{u} \cdot \nabla)v = -g' \frac{\partial h}{\partial y} - fu + \frac{1}{\rho h}\tau_y \quad (211)$$

$$\frac{\partial h}{\partial t} + \mathbf{u} \cdot \nabla h = -h \nabla \cdot \mathbf{u} \quad . \quad (212)$$

We have used h instead of h_1 for simplicity as the *thermocline depth*, and ρ instead of ρ_1 as density in the upper layer. It is quite instructive to consider the motionless stationary state of such a model (even in a more complex situation this may be a good approximation):

$$\frac{\partial h}{\partial x} = \frac{1}{\rho h g'}\tau_x \quad (213)$$

$$\frac{\partial h}{\partial y} = \frac{1}{\rho h g'}\tau_y \quad , \quad (214)$$

assuming a typical situation in the equatorial Pacific with purely easterly trade winds ($\tau_x < 0$, $\tau_y = 0$) it becomes clear why the equatorial Pacific thermocline is tilted from west to east!!!!

It is interesting to note that the (forcing) free Eq. (210) - (212) are formally identical to the shallow water equations 162, 163 and 167 that we used to derive the equatorial Rossby and Kelvin waves, if we replace g by g', the reduced gravity. This means that the reduced gravity equations support the same solutions as the shallow water equations near the equator, if we also in all phase velocities replace g by g'. We will see these kind of waves in the following example.

In the following we present and discuss the ocean adjustment to a constant atmospheric wind-stress forcing of the ocean derived from a model similar, but slightly more complicated than Eq. 210 - 212. The addition is basically an equation for the surface temperature that is not present in Eq. 210 - 212. In a strict sense, the surface temperature would never be influenced by the thermocline depth as long as this is positive. However, in the real world, there is a still a gradient present in the upper-layer, meaning that if the thermocline is nearer to the surface, the temperature is lower there, just as seen in Fig. 21. Furthermore, if temperature is allowed to vary horizontally then there will also be horizontal advection of temperature.

7.5 Ocean response to a zonal wind stress anomaly

Fig. 37 shows the wind-stress forcing applied with maximum at equator at 180 E, and a Gaussian shape of with 10 degrees in east-west and 5 degrees in north-south direction. The forcing is of magnitude 0.015 N/m^2, which is a typical response of the atmosphere to a typical ENSO anomaly. This forcing is mimiking the atmospheric Gill-response on the equator to the ENSO-induced heating (SST) anomaly. We are considering the time evolution of the thermocline response to the constant forcing.

Fig. 38a shows the response after the first month of forcing, and we see interestingly that the response resembles the Gill response that we discussed for the atmosphere to a diabatic heating anomaly, with an equatorial Kelvin wave to the east of the wind stress forcing and 2 Rossby waves struddling the equator to the west. The Kelvin wave signal moves to the east as time evolves and the Rossby wave signal moves to the west (as they should). The Kelvin waves reach the eastern boundary after about 4 month (Fig. 38b) and appear to transform into coastal Kelvin waves that move north- and southward from the equator. The maximum response is reached after about 6 month, and is then decaying somewhat. The stationary response is seen in Fig. 38f. The thermocline tilt in the steady-state solution seems to balance the wind-stress forcing, showing that Eqs. 213 are a good approximation.

Fig. 39 shows the corresponding response in sea surface temperatures (using an additional equation not present in Eq. (210) - (212)). Remember that the atmospheric forcing was mimicking the Gill-type response to a warm SST anomaly. From Fig. 39 we clearly identify that the ocean response to the atmospheric forcing provides a positive feedback: The SST in the eastern equatorial Pacific is further increased. The SST response evolves slower than the thermocline response (because the response starts in the central/western Pacific where the thermocline is relatively deep in the mean state and its fluctuations are therefore less coupled to the surface. The maximum positive feedback seems to occur after about 6 to 12 months and it decays to reach an equilibrium. This decay could be interpreted as the delayed negative feedback provided by the ocean to the ENSO phenomenon.

Exercises

1. Assume a mean wind stress distribution along the equator:

$$\begin{aligned} \tau_x &= 0 \quad \text{for lon} \leq 170 \text{ E} \\ \tau_x &= -0.06 \text{ N/m}^2 \quad \text{for } 170 \text{ E} \leq \text{lon} \leq 240 \text{ E} \\ \tau_x &= 0 \quad \text{for lon} \geq 240 \text{ E} \end{aligned} \tag{215}$$

   Using the approximation 213, calculate the thermocline distribution along the equator, assuming that the thermocline depth at the western edge is 150 m. What is the total change in height between 170 E and 240 E?

2. Calculate the oceanic Kelvin wave speed of (using the reduced gravity approximation) of an ocean with a mean thermocline depth of 100 m.

El Niño 2015/2016

Perhaps the strongest event in the recent history?

Dec 2015 – Mar 2016 SST anomalies

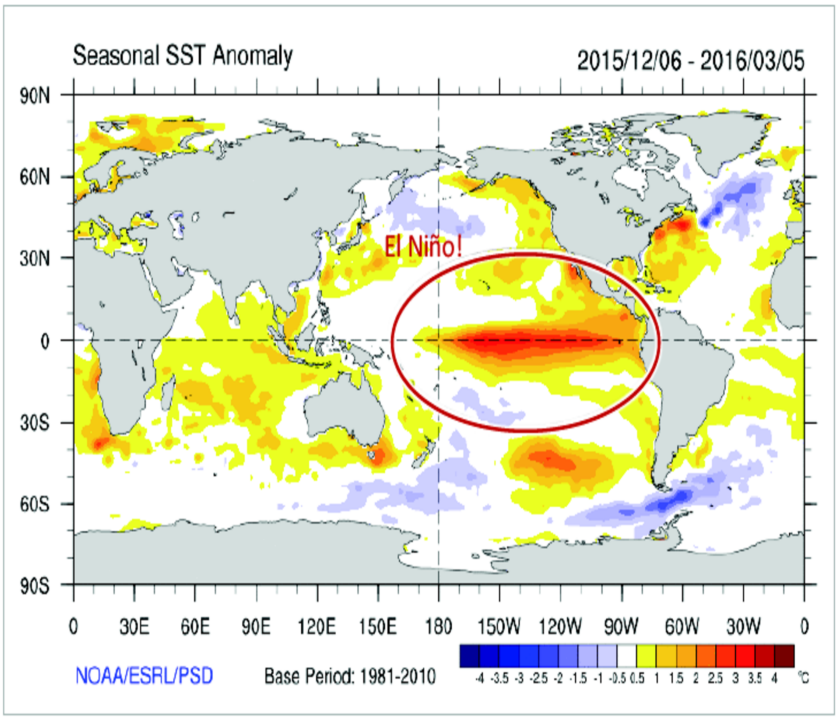

7

This slide, as many in the following from Bianca Mezzina's Master thesis defence

Figure 27: Sea Surface Temperature Anomalies in winter 2015/2016.

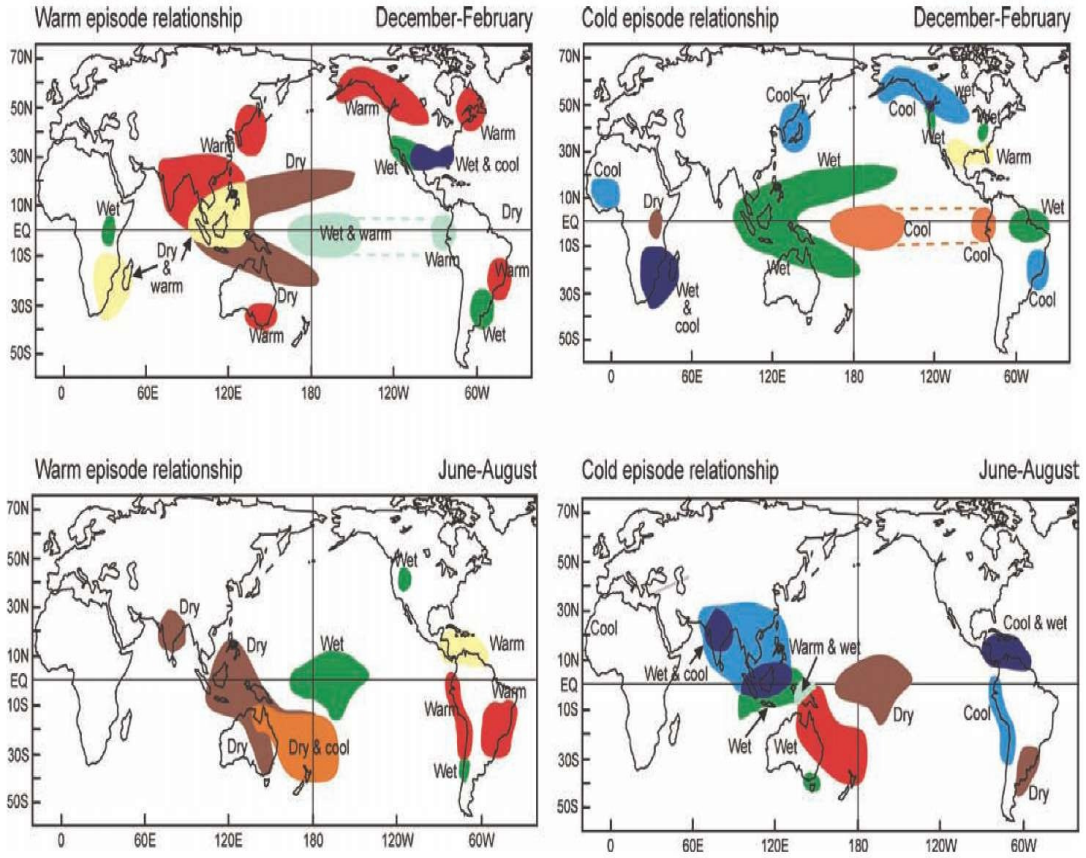

Figure 28: Some known ENSO teleconnections. Note that not all teleconnections are shown, only the most robust ones. Source: NOAA

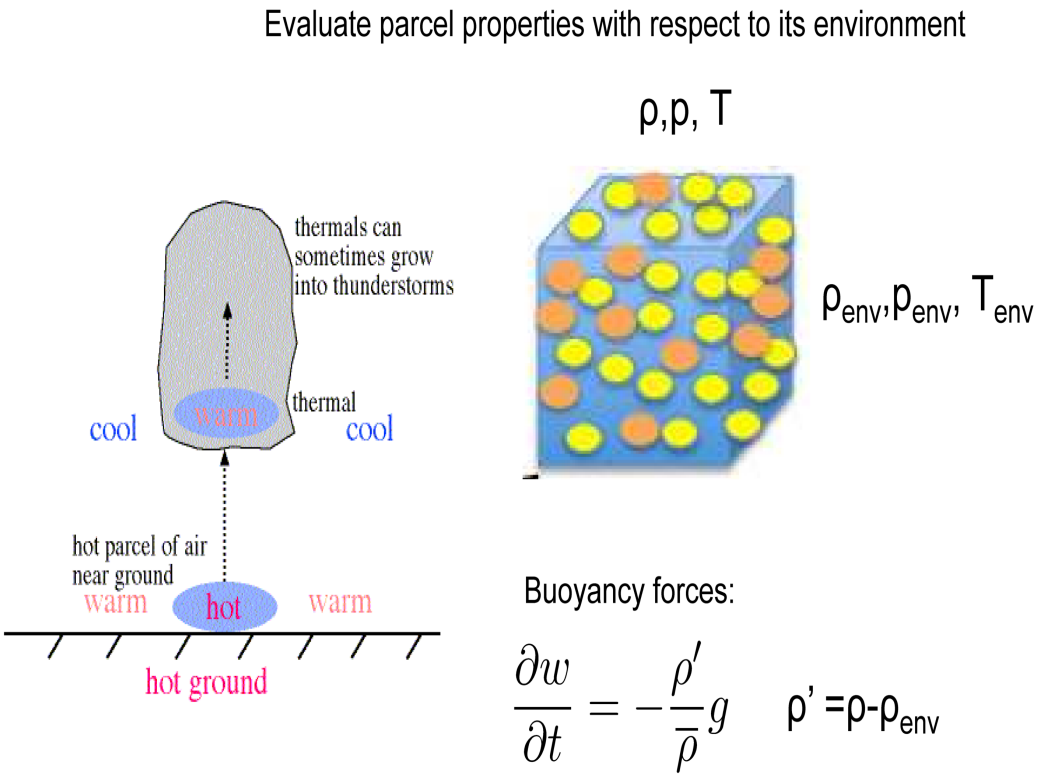

Figure 29: Sketch of a parcel in an environment that is warmed from below.

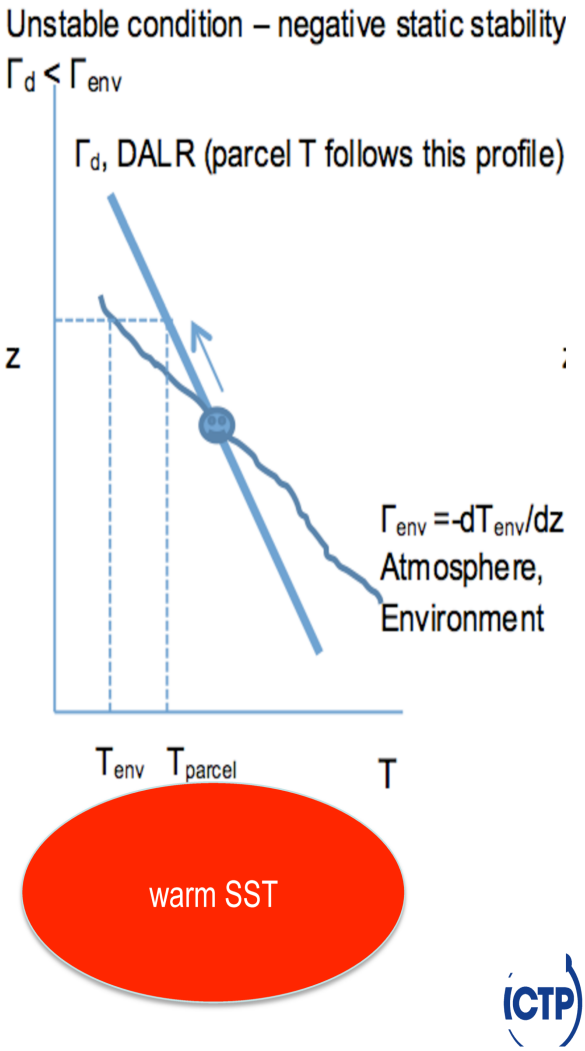

Figure 30: Sketch how the environment is favorable or unfavorable for convection and may be influenced by surface conditions.

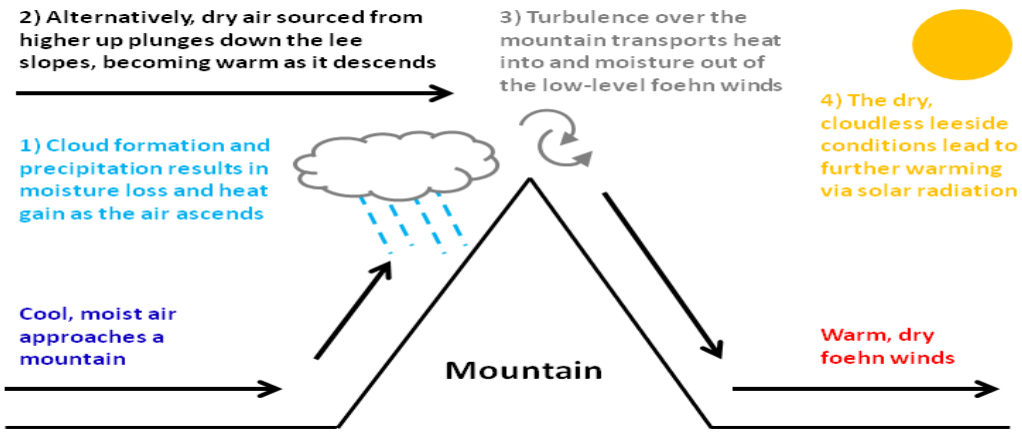

Figure 31: Foehn effect mechanism.

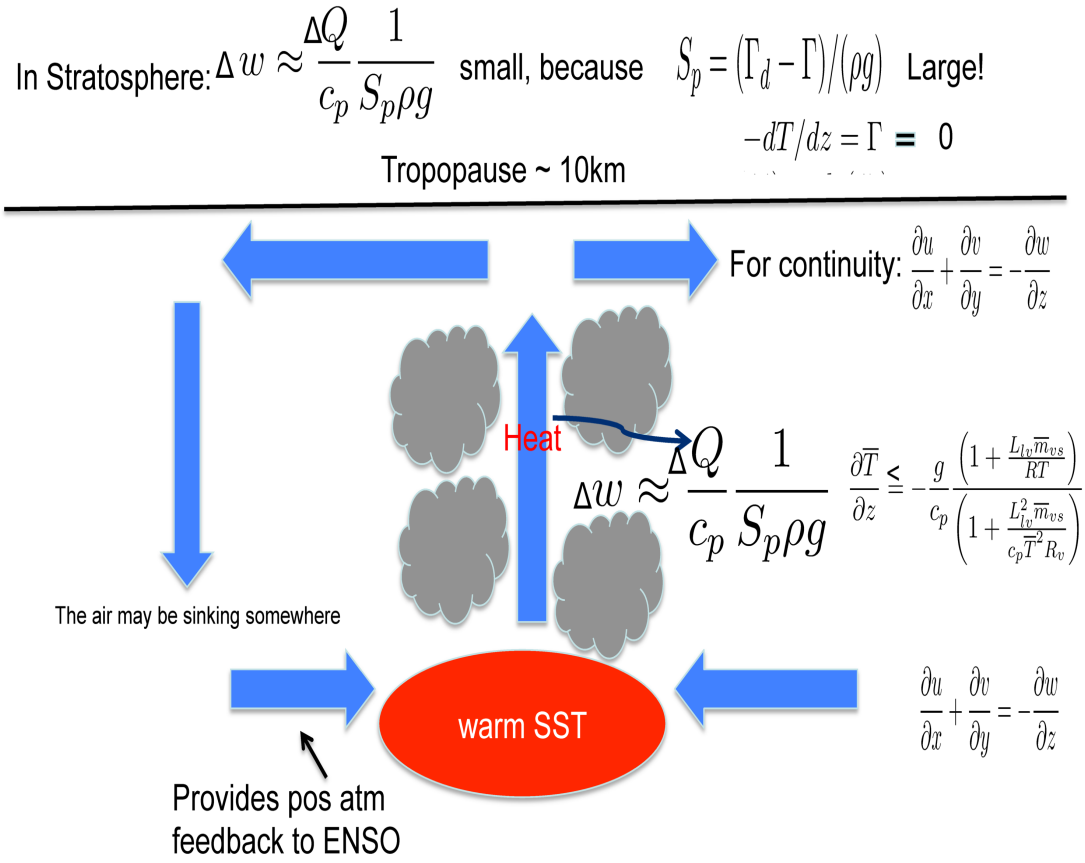

Figure 32: Large-scale adjustments to diabatic convective heating.

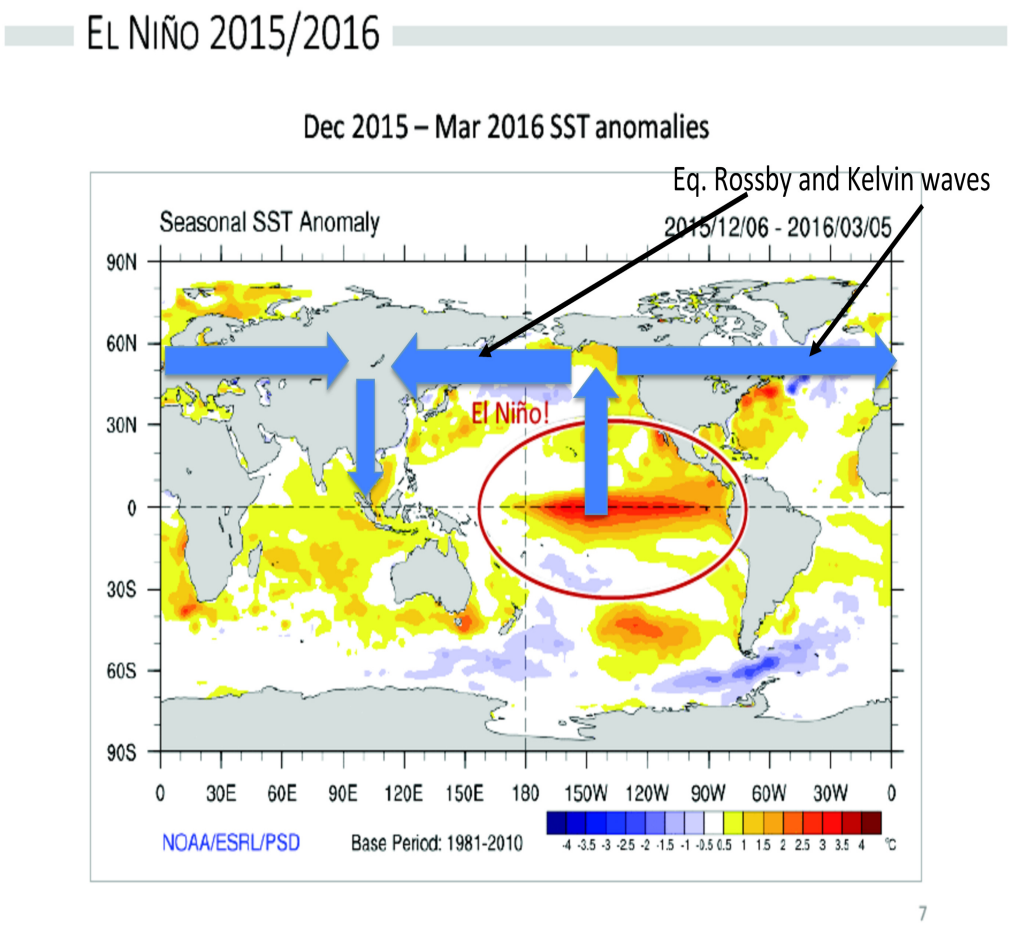

Figure 33: Large-scale adjustments to diabatic convective heating induced by ENSO.

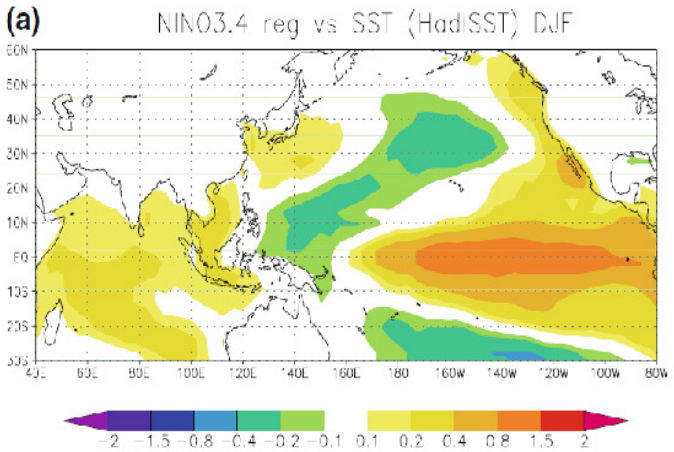

Figure 34: Composite sea surface temperature anomaly for an El Nino condition. Units are K.

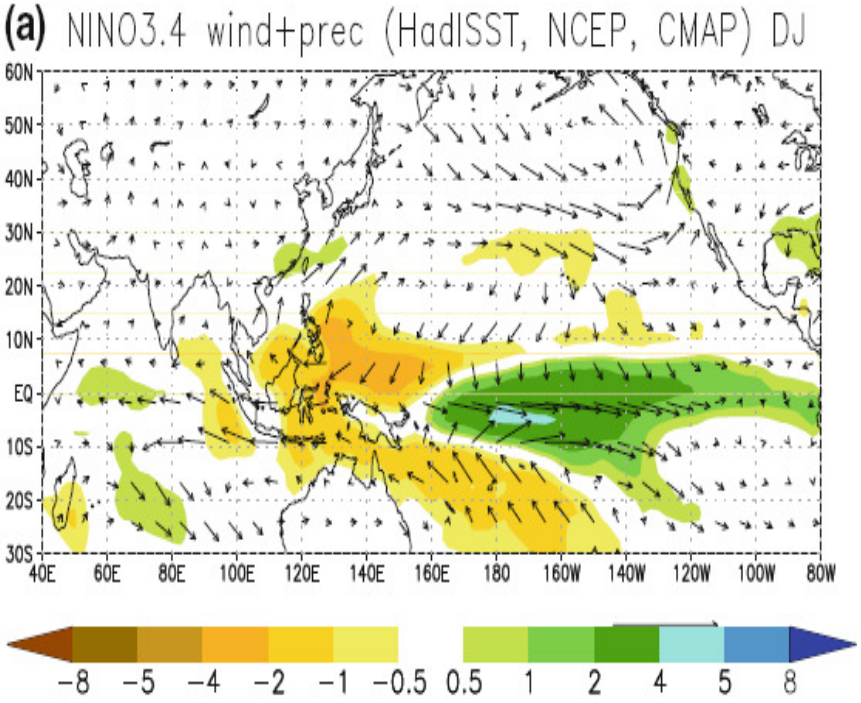

Figure 35: Composite of response to an El Nino forcing. Shading Precipitation in mm/day, vectors 925 hPa wind.

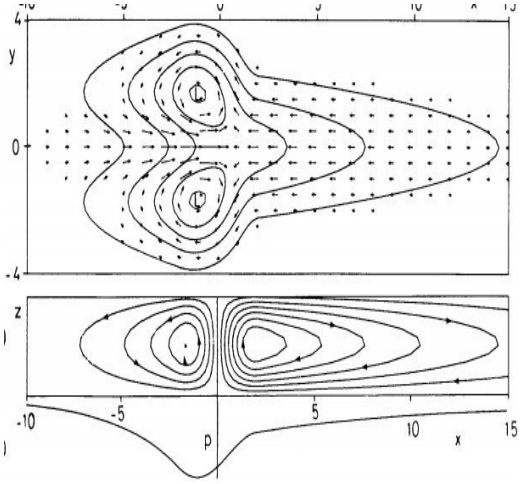

Figure 36: Illustration response to equatorial heating according to the gill model. Equatorial rossby waves shape the response to the west and Kelvin waves shape the response to the east

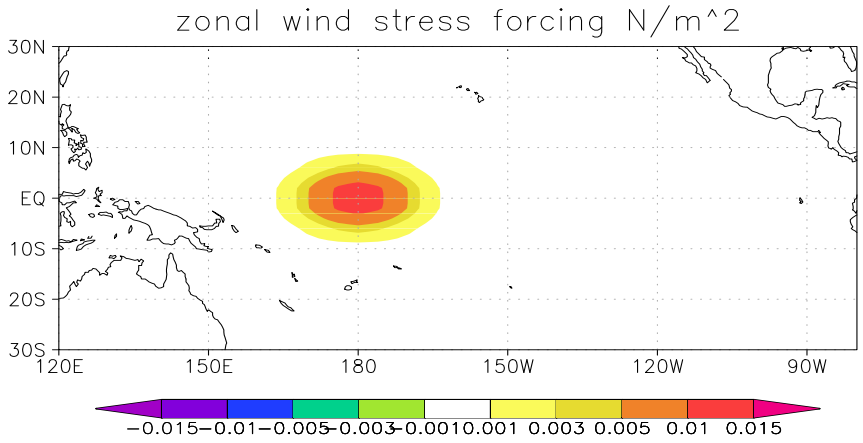

Figure 37: Zonal wind stress forcing. Units are N/m^2.

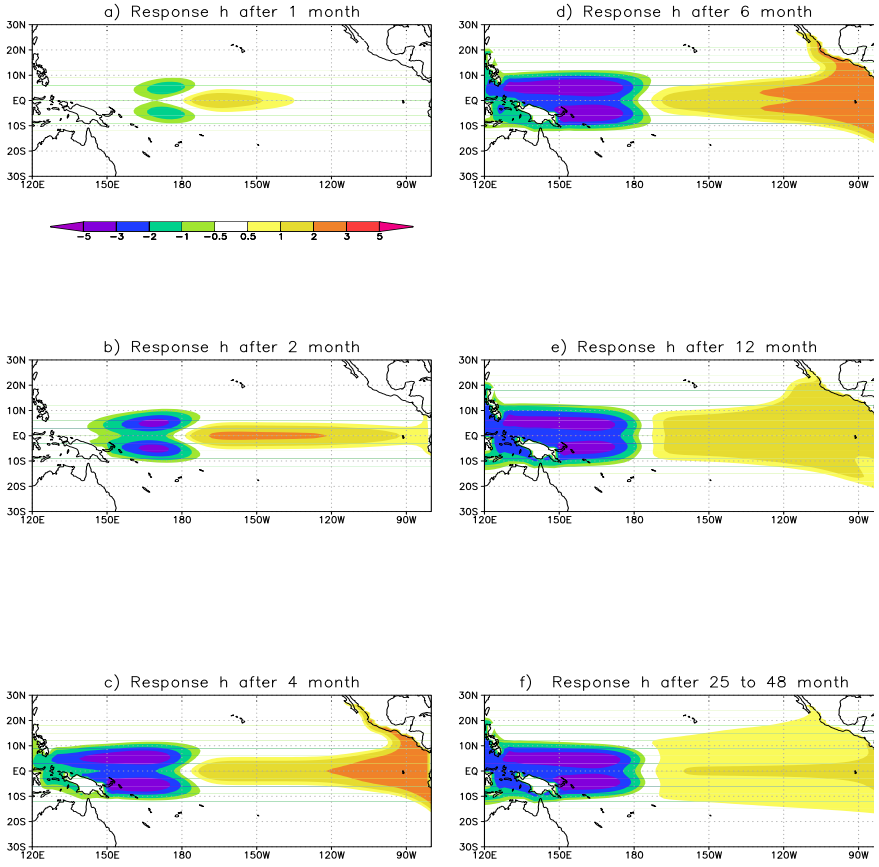

Figure 38: Thermocline response to anomalous zonal wind stress forcing of Fig. 37. a) after 1 month, b) after 2 months, c) after 4 months, d) after 6 months, e) after 12 months. f) stationary response. Units are m.

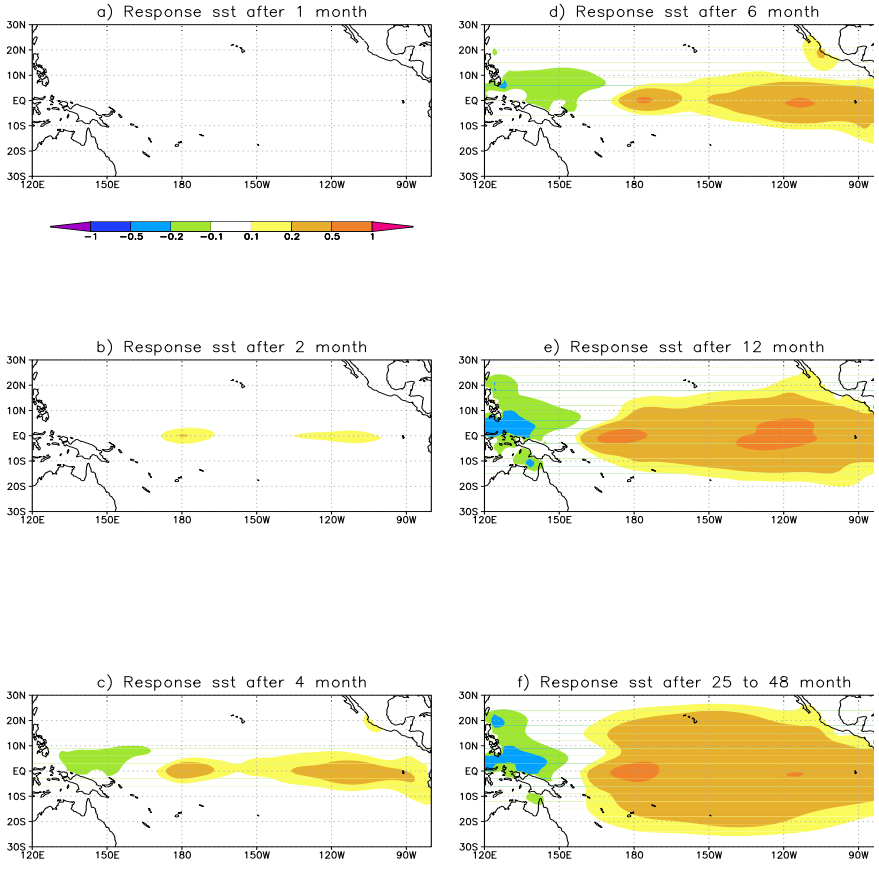

Figure 39: SST response to anomalous zonal wind stress forcing of Fig. 37. a) after 1 month, b) after 2 months, c) after 4 months, d) after 6 months, e) after 12 months. f) stationary response. Units are K.